Journal of Engineering and Applied Science Vol. 10, No. 02, pp. 53–62, June 2026

Journal of Engineering and Applied Science

Contents are available at www.jeas.ruet.ac.bd

Investigation of Mechanical Performance of Carbon Fiber Powder-Reinforced Composites through SLA-Based Additive Manufacturing

Md. Rubel Miah[1], Sovon Das[1], Rotan Kumar Saha[1*], Md. Kamal Hossen[1], Md. Polash Mia[1]

[1]*Department of Industrial and Production Engineering, Dhaka University of Engineering & Technology, Gazipur, Bangladesh*

ARTICLE INFORMATION

Received date: 19 May 2026
Revised date: 24 June 2026
Accepted date: 25 July 2026

Keywords

Mechanical properties
Additive manufacturing
Reinforced composites
Stereolithography (SLA)
Carbon fiber powder (CFP)

ABSTRACT

This study investigates the mechanical performance of carbon fiber powder (CFP)-reinforced photopolymer composites fabricated through stereolithography (SLA)-based additive manufacturing. Composite specimens containing 0-0.5 wt% CFP were fabricated and evaluated through tensile, hardness, surface roughness, SEM and particle analyses. The incorporation of CPF significantly improved the mechanical properties of the printed composites. The highest tensile strength of 13.04 MPa was achieved at 0.375 wt% CFP loading (S4), representing a substantial improvement over the neat resin specimen (5.83 MPa). Maximum hardness (58 HD) and the lowest surface roughness (Ra = 2.66 μm) were obtained at 0.5 wt% CFP content (S5). SEM and particle analyses revealed that excessive reinforcement promoted brittle fracture characteristics, internal cracking and increased surface irregularities. Overall, CFP contents between 0.25 and 0.375 wt% provided the best balance between strength, hardness and ductility. These findings demonstrate the potential of SLA-fabricated CFP composites for lightweight engineering and functional structural applications.

1. Introduction

Additive manufacturing (AM), commonly known as three-dimensional (3D) printing, has emerged as a transformative manufacturing technology capable of producing complex geometries through the layer-by-layer deposition of materials directly from computer-aided design (CAD) models [1]. Unlike conventional subtractive manufacturing, AM minimizes material waste, reduces tooling requirements and enables rapid fabrication of customized components. These advantages have accelerated its adoption across aerospace, automotive, biomedical, electronics and soft robotic applications, where lightweight structures and design flexibility are critical [2]. AM enables intricate internal structures and topology-optimized designs, significantly enhancing industrial relevance beyond traditional manufacturing limitations [3].Among the various AM technologies, vat photopolymerization-based processes such as stereolithography (SLA) and liquid crystal display (LCD) printing have attracted substantial attention because of their exceptional dimensional accuracy and superior surface finish SLA technology operates through the selective curing of liquid photopolymer resin using a focused ultraviolet (UV) laser beam, where the resin undergoes localized photopolymerization and solidifies layer-by-layer to form a three-dimensional object [4]

* Corresponding authors: Department of Industrial and Production Engineering, Dhaka University of Engineering & Technology, Gazipur, Bangladesh
E-mail addresses: rotansaha@duet.ac.bd (Rotan Kumar Saha, IPE, DUET)

Compared with extrusion-based techniques such as fused deposition modeling (FDM), SLA can achieve significantly finer layer resolutions and smoother surfaces typically ranging from 25 to 100 µm [5]. Despite these advantages, the widespread application of SLA-printed photopolymer materials in structural and load-bearing applications remains limited due to their inherent brittleness, low fracture toughness and relatively poor mechanical strength. Previous studies have reported that conventional SLA resins possess tensile strengths in the range of 25-55 MPa, which are considerably lower than those required for many advanced engineering applications. Furthermore, weak interlayer adhesion and residual porosity generated during the curing process can further deteriorate structural reliability and dimensional stability [6]. To overcome the inherent brittleness and limited structural performance of SLA photopolymer resins, recent studies have explored reinforcement using micro and nano-scale fillers to enhance mechanical integrity. Among various reinforcements, including glass and Kevlar fibers, CFP has attracted significant attention due to its high specific strength (>3 GPa tensile strength), high elastic modulus (200-700 GPa), low density and superior fatigue resistance. Incorporating CFP into photopolymer matrices has been reported to enhance tensile strength, hardness, stiffness and dimensional stability while preserving lightweight characteristics. However, most existing studies primarily focus on isolated mechanical responses, with limited correlation to microstructural evolution and surface integrity. The novelty of the present work lies in a comprehensive evaluation of CFP-reinforced SLA composites by correlating mechanical behavior with surface roughness, SEM morphology and quantitative particle analysis to identify an optimal reinforcement range for balanced performance [7].

Salih, Raveen Mohammed, et al. investigated carbon fiber-reinforced photopolymer composites fabricated using LCD-based printing technology and evaluated the effects of carbon fiber loading (0-0.5 wt %) and layer thickness (30-50 µm) on tensile properties. Their results demonstrated that the incorporation of 0.25 wt% carbon fiber with a 30 µm layer thickness increased tensile strength by approximately 47.8% compared with neat resin specimens. However, when the carbon fiber content increased to 0.5 wt%, the tensile strength deteriorated due to fiber agglomeration, void formation and weak interfacial bonding between the fiber and resin matrix [8]. Similarly, Gao, Tianyu, et al. conducted a systematic investigation on Kevlar fiber-reinforced flexible photopolymer composites fabricated using SLA technology. Their study examined the combined effects of layer thickness (0.05 and 0.10 mm) and printing orientation on tensile behavior, hardness and surface quality. The optimized specimen consisting of 90 wt% elastic resin, 9.8 wt% standard resin, and 0.2 wt% Kevlar fiber exhibited a maximum tensile stress of 7.27 MPa and an elongation at break of 161.6% when printed at 0.05 mm layer thickness in flat orientation. In addition, Kevlar reinforcement improved surface quality and increasing hardness up to 34.38 Shore D [9]. Xiao R. et al. explored the effect of short carbon fiber reinforcement on the mechanical properties of SLA-printed photopolymer composites. The study reported that incorporating low concentrations of carbon fiber significantly improved tensile strength, flexural modulus and hardness of the printed components due to enhanced load transfer between the fiber and resin matrix. The authors observed that specimens reinforced with approximately 0.3 wt% carbon fiber exhibited the best mechanical performance, with tensile strength increasing by nearly 35% compared with pure resin samples [10]. In another study, Ramesh M. et al. examined the influence of printing orientation and layer thickness on the mechanical and surface characteristics of carbon fiber-reinforced photopolymer composites produced using SLA technology. Their results demonstrated that specimens printed with thinner layers and flat orientation showed superior tensile and flexural properties because of improved interlayer adhesion and reduced anisotropic defects. The optimized composite samples achieved approximately 28% higher tensile strength and significantly lower surface roughness compared with vertically printed specimens [11].

Critical evaluation of previous studies reveals that the performance of SLA-printed composites is governed by reinforcement content, layer thickness, print orientation, fiber distribution and interfacial bonding. While reduced layer thickness enhances interlayer cohesion and structural uniformity, excessive filler loading promotes agglomeration, void formation, and stress concentrations, ultimately degrading mechanical reliability [12]. Although previous studies have demonstrated promising improvements in mechanical behavior, inconsistencies in fiber distribution, curing efficiency and interfacial compatibility remain major challenges for achieving reproducible and reliable performance [13]. Most available studies also primarily focus on flexible resin systems, LCD-based printing or low reinforcement concentrations, while comprehensive investigations on CFP-reinforced standard resin composites fabricated specifically through SLA-based additive manufacturing remain limited [14]. The relationship between fiber loading and defect formation mechanisms such as porosity, interfacial debonding and anisotropic failure has not yet been systematically clarified [15].

These limitations indicate a significant research gap in developing mechanically robust SLA-fabricated CFP composites suitable for functional engineering applications. Therefore, the primary aim of the present study is to investigate the mechanical performance of CFP-reinforced composites fabricated through SLA-based additive manufacturing. The specific objectives of this research are: (i) to fabricate CFP-reinforced standard resin composites using SLA technology, (ii) to evaluate the influence of CFP incorporation on tensile strength, hardness and structural behavior, (iii) to analyze the microstructural characteristics particles analysis and interfacial bonding mechanisms responsible for mechanical performance and (iv) to identify the relationship between reinforcement distribution and defect formation in SLA-fabricated composites. The findings of this study are expected to contribute toward the development of lightweight, high-strength photopolymer composites for advanced engineering and functional manufacturing applications.

2. Materials and methodology

2.1 Materials

In the present study, an acrylic-based flashforge standard photopolymer resin and carbon fiber powder (CFP) were employed as the matrix and reinforcing materials, respectively, for the fabrication of composite specimens using SLA-based additive manufacturing. The acrylic-based photopolymer resin was selected due to its excellent printability, dimensional accuracy, rapid UV-curing capability and strong compatibility with stereolithography (SLA) processes. In addition, the resin provides adequate interlayer adhesion, surface quality and structural integrity during layer-by-layer fabrication, making it suitable for high-resolution printed components. CFP was incorporated as a reinforcing filler to enhance the mechanical performance and stiffness of the photopolymer matrix while maintaining the geometric precision achievable through SLA printing. However, neat photopolymer resins generally exhibit brittle behavior, limited toughness and comparatively lower mechanical strength, which restrict their use in high-load engineering applications [17]. To improve the stiffness and strength of the printed composites, conductive reinforced CFP with a particle size of 100 mesh (approximately 150 µm) was used as the reinforcing filler. CFP possesses outstanding mechanical and physical properties including excellent thermal and chemical stability. Table 1 presents the properties of standard photopolymer resin and CFP, while Figure 1 illustrates the composite formulations. CFP is an effective reinforcement for lightweight, high-performance composites and has been reported to enhance hardness, dimensional stability, wear resistance and thermal conductivity in photopolymer-based materials [18]. In this research, CFP was incorporated into the acrylic-based standard resin matrix to investigate its influence on the mechanical performance and structural behavior of SLA-fabricated composite specimens.

Table 1. Properties of standard photopolymer resin and carbon fiber powder.

Material	Property	Typical Value	Units
Standard Photopolymer Resin	Tensile Strength	23-52	MPa
	Elastic Modulus	1.5-3.0	GPa
	Elongation at Break	12-6.2	%
	Flexural Modulus	1.25-2.2	GPa
	Printing Resolution	25-100	µm
	Density	1.10–1.20	g/cm
Carbon fiber powder (CFP)	Tensile Strength	4-5	GPa
	Elastic Modulus	200-700	GPa
	Density	1.8-2.2	g/cm
	Particle Size	100-150	µm
	Color	Black	-

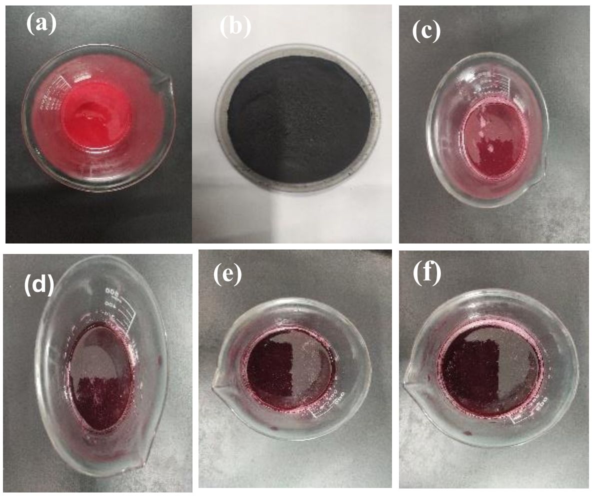

Figure 1. Materials and composite formulations used in this study: (a) standard photopolymer resin, (b) carbon fiber powder (CFP), (c) standard resin (99.875 wt%) reinforced with CFP (0.125 wt%), (d) standard resin (99.75 wt%) reinforced with CFP (0.25 wt%), (e) standard resin (99.625 wt%) reinforced with CPF (0.375 wt%), and (f) standard resin (99.5 wt%) reinforced with CFP (0.5 wt%).

2.2 Experimental design and parameter setup

The experimental design was developed to investigate the influence of CFP content on the mechanical and surface properties of SLA-fabricated photopolymer composites. Five formulations containing 0-0.5 wt% CFP were selected based on preliminary trials and literature recommendations to minimize excessive viscosity, particle agglomeration and curing instability commonly associated with higher filler loadings. Standard dog-bone tensile specimens were designed using CAD software in accordance with ASTM D638 requirements, as illustrated in Figure 2. This geometry ensures uniform stress distribution within the gauge section and provides reliable tensile property measurements [19].

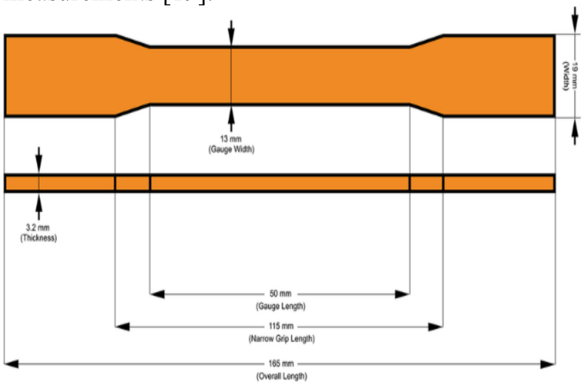

Figure 2. Testing specimen dimension according to ASTM D638.

The CAD models were exported in STL format and processed using slicing software prior to fabrication. Printing parameters, including layer thickness (0.1mm), build orientation (flat), bottom layers (5 layers) and normal exposure time (2.5s), were carefully configured to ensure dimensional accuracy and repeatability. All specimens were fabricated under identical SLA processing conditions to isolate the effect of CFP concentration on material performance. The overall experimental workflow, including material preparation, specimen design, SLA printing, post-curing, mechanical testing, surface characterization, SEM examination and particle analysis is presented in Figure 3.

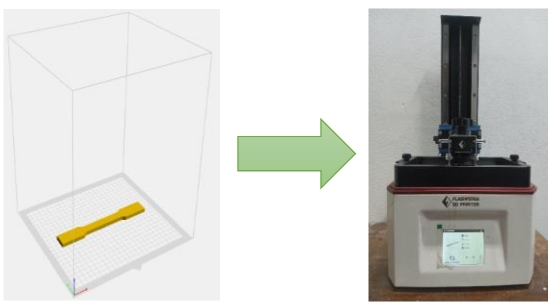

Figure 3. Parameters set up in slice software and the SLA 3D printer.

2.3 Materials composition and 3D printing process

CFP was incorporated into the acrylic-based standard photopolymer resin at concentrations of 0.125, 0.25, 0.375 and 0.5 wt%, while the neat resin specimen served as the control sample. The detailed formulations and printing parameters are summarized in Table 2. Prior to printing, the required amount of CFP was gradually added to the resin and mechanically stirred for a predetermined 5min duration to achieve homogeneous particle distribution. The mixture was subsequently degassed to minimize air entrapment and reduce the likelihood of particle agglomeration and void formation.

Table 2. Composition and printing parameters of samples prepared for the SLA 3D printing process.

Sample No.	Standard Resin (wt %)	Carbon Fiber Powder (wt %)	Layer Thickness (mm)	Total Weight (wt %)	Printing Position
S1	100	0	0.1	100	Flat
S2	99.875	0.125	0.1	100	Flat
S3	99.75	0.25	0.1	100	Flat
S4	99.625	0.375	0.1	100	Flat
S5	99.50	0.5	0.1	100	Flat

The prepared resin-CFP suspensions were fabricated using an SLA 3D-printing system under identical processing conditions, including a layer thickness of 0.1 mm and flat build orientation, ensuring a reliable comparison among specimens. Following slicing and parameter setup, the specimens were produced through layer-by-layer UV-induced photopolymerization. After fabrication, all samples were cleaned with isopropyl alcohol to remove uncured resin and subsequently post-cured under UV irradiation at 20min to ensure complete polymerization and dimensional stability. The overall fabrication, characterization and testing procedure is illustrated in the experimental workflow presented in Figure 3.

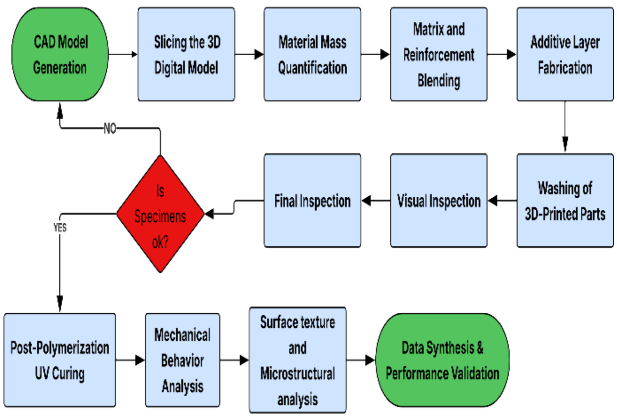

Figure 4. Experimental process flow diagram of SLA 3D printed samples.

Figure 5 shows a representative test specimen fabricated using the SLA 3D printer in this study, following the layer-by-layer slicing process. The printed part exhibits a smooth flat surface finish and the incorporation of CFP (ranging from 0 to 0.5 wt %) into the standard resin is visibly uniform across the layers.

Figure 5. SLA 3D printed specimen prepared with varying compositions of standard resin and CFP (as listed in Table 2).

3. Results and discussion

In this section presents a comprehensive analysis of the mechanical and physical properties of the SLA 3D-printed standard resin composites reinforced with CFP. The discussion focuses on key parameters, including tensile strength, modulus of elasticity, surface roughness, percentage of elongation, hardness, surface roughness, scanning electron microscopy (SEM) and particle analysis, which are crucial for evaluating the suitability of these materials.

3.1 Tensile properties analysis

The tensile properties of the fabricated samples were evaluated to characterize their mechanical behavior. Table 3 summarizes the tensile test results for the five samples, conducted at a constant crosshead speed of 5 mm/min. The maximum recorded forces ranged from 275.37 N to 565.72 N, corresponding to ultimate tensile stresses between 5.83 Mpa and 13.04 MPa. The peak strain values varied from 9.71% to 16.57%, indicating moderate ductility across the specimens. Among the samples, Sample 4 exhibited the highest tensile strength, whereas Sample 1 demonstrated the lowest.

Table 3. Ultimate Tensile properties test Result.

Sample No.	Speed (mm/min)	Max Forces (N)	Stress (MPa)	Strain (%)
S1	5	275.37	5.83	11
S2	5	491.52	10.28	16.57
S3	5	565.72	11.82	14.34
S4	5	507.78	13.04	9.71
S5	5	502.78	12.4	12.41

Figure 6 illustrates the tensile stress-strain behavior of SLA-fabricated standard resin composites reinforced with varying concentrations of CFP. The results demonstrate that CFP incorporation substantially improves the tensile performance of the photopolymer matrix. The neat resin specimen (S1) exhibited the lowest tensile strength of 5.83 MPa with a strain of 11%, reflecting its inherently brittle nature and limited load-bearing capability. The addition of CFP significantly enhanced strength, with tensile stress increasing to 10.28 MPa for S2 (0.125 wt%) and 11.82 MPa for S3 (0.25 wt%). This improvement can be attributed to more effective stress transfer from the matrix to the reinforcing particles and increased resistance to crack initiation. The optimum mechanical performance was achieved by S4 containing 0.375 wt% CFP, which exhibited the highest tensile strength of 13.04 MPa, representing an improvement of approximately 124% compared with the unreinforced resin. This enhancement is associated with favorable particle dispersion and stronger interfacial interactions between the CFP and the cured resin matrix. However, a slight reduction in strength was observed for S5 (12.40 MPa) at 0.5 wt% CFP. This decline is likely related to particle agglomeration, increased resin viscosity and localized curing irregularities, which can promote defect formation and reduce stress-transfer efficiency. These findings indicate that 0.375 wt% CFP represents the optimum reinforcement level for maximizing tensile performance in SLA-printed photopolymer composites.

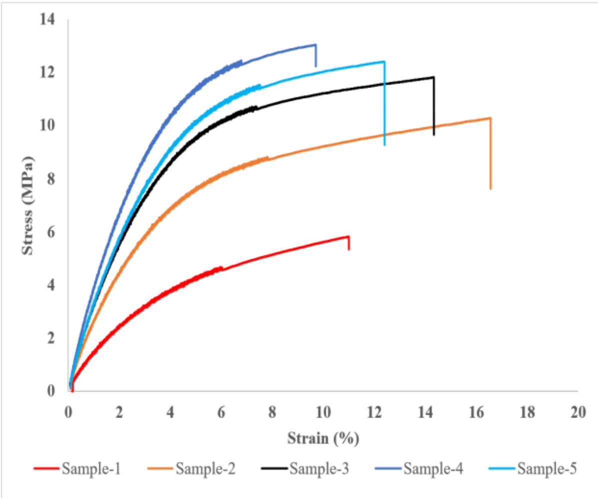

Figure 6. Strain vs. Strain Curve of the 3D printed specimens.

Figure 7 presents the variation in tensile strength and elastic modulus of SLA-printed composites (S1-S5) with increasing CFP content. Both mechanical properties show a consistent improvement from S1 to S4, followed by a slight reduction at S5. The tensile strength increases significantly from 5.83 MPa for the neat resin (S1) to a maximum of 13.04 MPa at 0.375 wt% CFP (S4), before decreasing marginally to 12.40 MPa at 0.5 wt% (S5). Similarly, the elastic modulus rises from 52.89 MPa (S1) to 134.39 MPa (S4), then decreases to 100 MPa at S5. This behavior indicates that moderate CFP incorporation enhances load transfer efficiency and stiffness due to improved reinforcement dispersion and interfacial interaction. However, excessive CFP loading likely induces particle agglomeration and localized stress concentration, leading to reduced mechanical efficiency beyond the optimal composition.

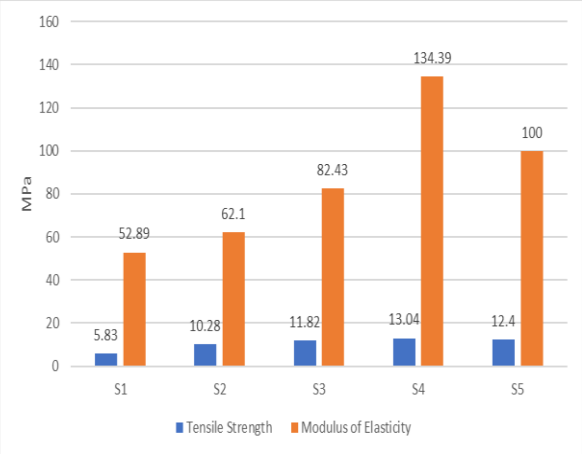

Figure 7. Trending of tensile strength and modulus of elasticity of the specimens.

3.2 Hardness Test analysis

The Shore D hardness results demonstrate a progressive improvement in surface resistance with increasing CFP content, as presented in Table 4 and Figure 8, following the ASTM D2240 standard. The unreinforced resin specimen (S1) exhibited the lowest hardness value of 47.50 HD. The incorporation of CFP enhanced hardness consistently, reaching 50.50 HD for S2 (0.125 wt %) and 53.33 HD for S3 (0.25 wt %), representing a 12.3% increase relative to the neat resin. A further increase in reinforcement to 0.375 wt% (S4) produced a hardness of 54.33 HD, indicating a gradual stabilization of the reinforcing effect. The highest hardness value of 58.00 HD was obtained for S5 containing 0.5 wt% CFP, corresponding to an improvement of approximately 22.1% compared with S1. This enhancement is attributed to the intrinsic stiffness of carbon fiber particles and their ability to restrict localized deformation under indentation loading.

Table 4. Shore D hardness test results.

Sample No.	Point-1	Point-2	Point-3	Average Hardness (HD)
S1	48	47	47.5	47.50
S2	50	51	50.5	50.50
S3	54.5	53	52.5	53.33
S4	52.5	53.5	55	54.33
S5	58	56	60	58.00

These results clearly indicate that increasing CFP content enhances the composite's resistance to surface indentation and deformation under load. The improvement is attributed to the uniform dispersion of carbon powder particles within the resin matrix, which restricts polymer chain mobility and promotes stronger interfacial bonding between the reinforcement and the matrix. However, the hardness increment between S3 and S4 was relatively modest, possibly due to partial powder agglomeration at higher concentrations, which can reduce the uniformity of stress transfer. Overall, the trend confirms that CFP reinforcement effectively improves the surface hardness, mechanical durability and wear resistance of SLA-printed composites, as shown in Figure 8.

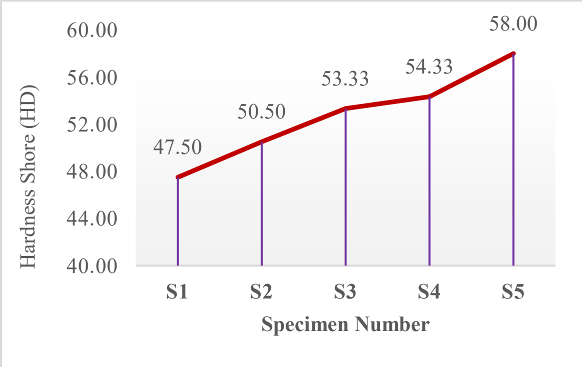

Figure 8. Trending hardness of the fabricated specimens.

3.3 Surface Roughness analysis

Surface roughness was measured using a Surtronic S-128 (Taylor & Hobson) following ISO 4287:1997 standards. The surface roughness parameters Ra (average roughness), Rq (root mean square roughness) and Rz (average maximum height) were measured for samples S1 to S5 to evaluate the effect of CFP content on surface finish. The results are summarized in the table 5 below and Figure 9 presents a comparative bar chart of the three roughness parameters.

Table 5. Surface roughness test results.

Sample No.	Ra (µm)	Rq (µm)	Rz (µm)
S1	3.19	3.75	13.74
S2	3.22	3.89	15.65
S3	3.22	3.80	14.30
S4	3.34	3.87	14.38
S5	2.66	3.08	12.64

The neat resin specimen (S1) exhibited moderate roughness values (Ra = 3.19 µm, Rq = 3.75 µm and Rz = 13.74 µm). A slight increase in roughness was observed for S2 (0.125 wt% CFP), which may be attributed to localized disturbances in resin flow and curing behavior induced by the dispersed particles. Specimens S3 and S4 displayed comparable roughness parameters, indicating relatively stable surface formation and homogeneous filler distribution. Interestingly, the highest CFP loading (0.5 wt%, S5) produced the lowest roughness values (Ra = 2.66 µm, Rq = 3.08 µm and Rz = 12.64 µm), suggesting a smoother external surface. However, SEM observations revealed the presence of internal cracks and subsurface defects, indicating that improved surface finish does not necessarily correspond to enhanced structural integrity.

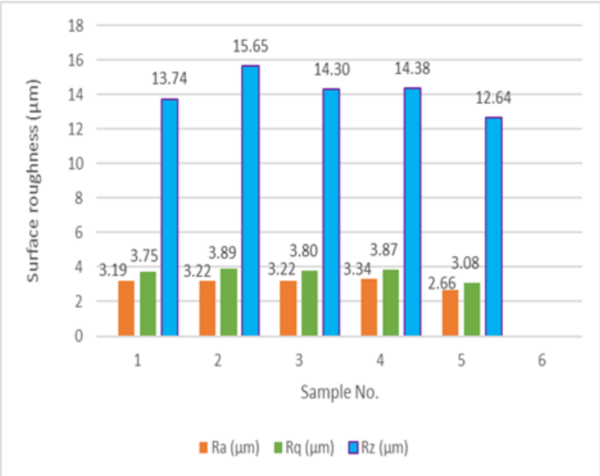

Figure 9. Surface roughness parameters (Ra, Rq, and Rz) of SLA-printed specimens S1 to S5 with increasing CFP (0–0.5 wt %).

3.4 Scanning electron microscopy (SEM) analysis

The surface morphology of the SLA-fabricated composites (S1-S5) was investigated using scanning electron microscopy, as shown in Figure 10, to evaluate the influence of carbon fiber powder (CFP) reinforcement on microstructural integrity. The analysis was performed at a magnification of 500 µm under an accelerating voltage of 15 kV, with optimized working distance to capture detailed surface features. The neat resin specimen (S1) exhibited noticeable excess resin accumulation and non-uniform surface regions, indicating heterogeneous curing and material distribution, which may act as potential stress concentration sites. In S2, the presence of distinct microvoids was observed, likely caused by entrapped air during layer-by-layer photopolymerization, leading to weakened local bonding and reduced structural continuity. Specimen S3 showed a combination of microvoids and uneven layer deposition, suggesting incomplete interlayer fusion and printing-induced defects that compromise mechanical uniformity. In S4, fracture features and crack propagation paths were evident, indicating a transition toward brittle failure behavior under tensile loading, where crack growth occurred along weak interfacial regions with limited plastic deformation. S5 showed subsurface cracking and internal damage; despite lowest surface roughness, defects arose due to higher CFP-induced agglomeration, curing heterogeneity, and reduced UV penetration during SLA processing. Overall, the SEM observations confirm that defect evolution including resin agglomeration, void formation, layer irregularities, and cracking plays a crucial role in governing the mechanical response and failure behavior of SLA-printed CFP-reinforced photopolymer composites.

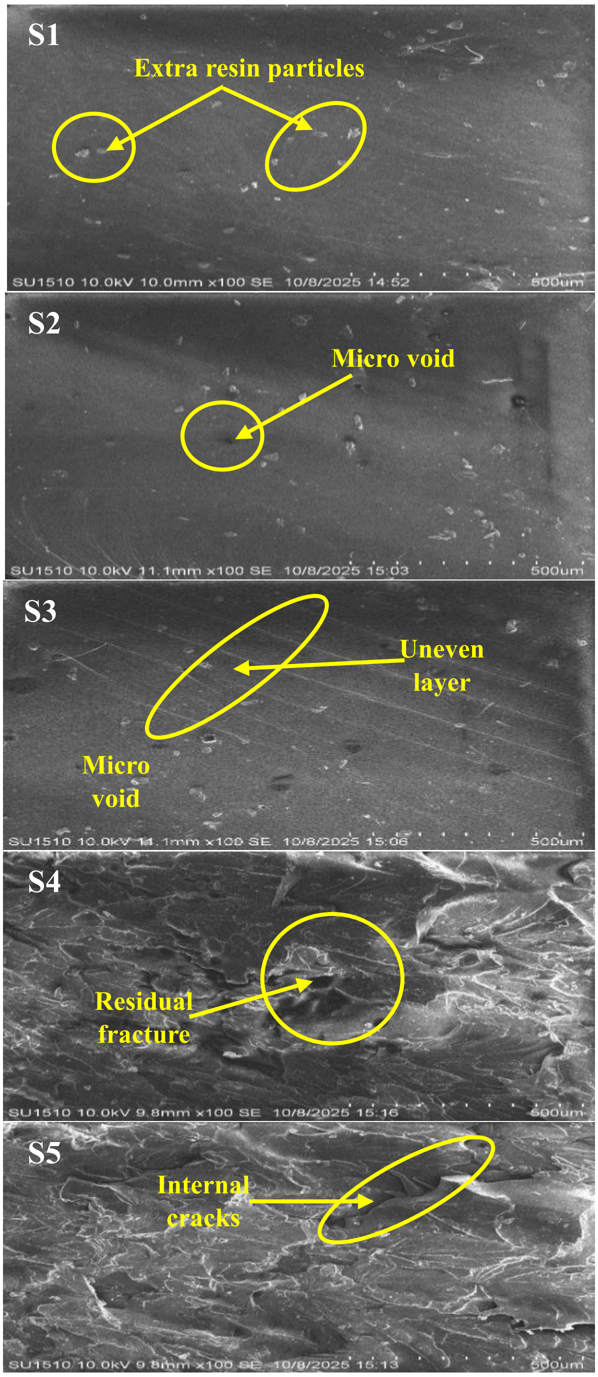

Figure 10. SEM micrographs of SLA 3D- printed standard resin composites reinforced with CFP.

3.5 Particle analysis

Quantitative particle analysis of SEM topography images for S1-S5 specimens was performed using Mountains® software with threshold-based detection (Figure 11). Key parameters, including particle count, surface coverage, particle density, individual particle area and maximum height (Z-max), were evaluated to investigate the influence of CFP content on surface morphology and microstructural uniformity. Specimens S1 and S2 exhibited comparable surface coverage, indicating relatively uniform surface distributions despite differences in CFP content. For S1, 394 particles were detected, corresponding to a surface coverage of 49.81% and a particle density of 3.263×10^{-4} particles/µm². The identified particle classes showed areas of 9813, 64,301, and 3989 µm² with corresponding Z-max values of 2.357, 2.499 and 1.990 µm, respectively. The global mean particle area and mean Z-max were 1.530 µm² and 1.463 µm. These characteristics indicate a relatively homogeneous surface morphology with limited topographical variation. In comparison, S2 contained 407 particles with a similar surface coverage of 49.99% and a slightly higher density of 3.710×10^{-4} particles/µm². The particle classes exhibited areas of 17,444, 846.7, and 272,178 µm², while the corresponding Z-max values ranged from 1.772 to 3.073 µm. The global mean particle area increased substantially to 1486 µm², whereas the mean Z-max remained relatively low at 1.625 µm. This behavior suggests the formation of larger surface features without a significant increase in surface relief, indicating acceptable particle dispersion and stable microstructural uniformity at low CFP loading.

Specimen S3 demonstrated a reduction in particle count (n = 374) with a coverage of 49.59% and a density of 3.097×10^{-2} particles/µm². Particle classification revealed: Particle 1 (area = 769.2 µm², Z-max = 228.8 nm), Particle 2 (area = 79.47 µm², Z-max = 248.5 nm), and an unlisted third class contributing additional variance. Global mean area was 16.04 µm², with a mean Z-max of 161.0 nm. The substantially lower Z-max values (consistent with nanometer-scale relief) relative to S1-S2 indicate a distinct surface regime, interpreted as uneven layer formation during printing rather than discrete particle protrusions. On the other hand, specimen S4 recorded 352 particles with a coverage of 49.61% and a density of 2.915×10^{-2} particles/µm². The identified particle classes were: Particle 1 (area = 30.84 µm², Z-max = 330.1 nm), Particle 2 (area = 3415 µm², Z-max = 358.3 nm) and Particle 3 (area = 20.61 µm², Z-max = 265.3 nm). The global mean area was 17.05 µm² and the mean Z-max was 201.0 nm. The combination of elevated Z-max across all classes and moderate coverage is consistent with a brittle fracture-dominated surface morphology. Specimen also S5 exhibited identical particle count (n = 352) and coverage (49.61%) to S4, with a density of 2.915×10^{-2} particles/µm². Three particle classes were identified: Particle 1 (area = 11.28 µm², Z-max = 334.8 nm), Particle 2 (area = 1763 µm², Z-max = 392.3 nm), and Particle 3 (area = 3.198 µm², Z-max = 297.2 nm). The global mean area remained 17.05 µm², while the mean Z-max reached the highest value among all specimens at 287.8 nm. The combination of the highest mean Z-max with minimal particle areas strongly suggests subsurface structural damage and internal crack propagation manifesting at the surface.

Across specimens S1 to S5, a progressive increase in mean Z-max was observed, accompanied by variable particle coverage and density. Specimen S1 exhibited the most uniform and topographically moderate surface characteristics. In contrast, S3, S4 and S5 displayed distinct surface relief signatures associated with uneven layer formation, brittle fracture and internal cracking, respectively. These results collectively demonstrate that CFP concentration and associated process parameters critically influence microstructural integrity and surface topography in SLA-printed composites, providing quantitative thresholds for defect mitigation and process optimization.

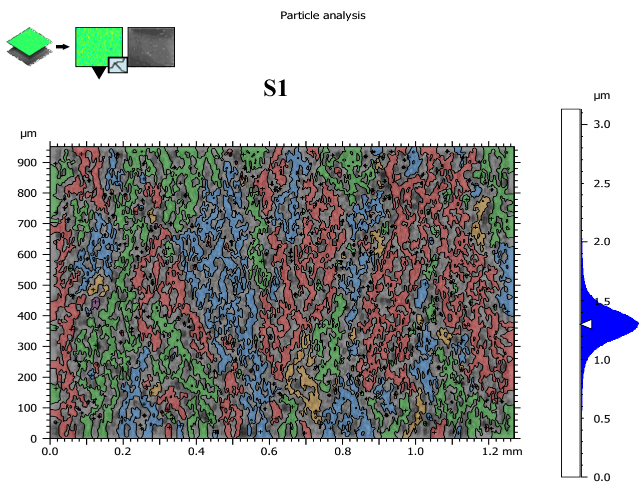

Information		
Method	Threshold detection	
Channel	Topography channel	
Number of particles	394	
Coverage	49.81	%
Density	0.0003263	Particles/µm²
Density (in pixels)	0.0004008	Particles/pixel²

Individual results		
Parameters	Area	Z-maximum
Unit	µm²	µm
Particle 1	9813	2.357
Particle 2	64301	2.499
Particle 3	3989	1.990
Global statistics		
Mean	1530	1.463

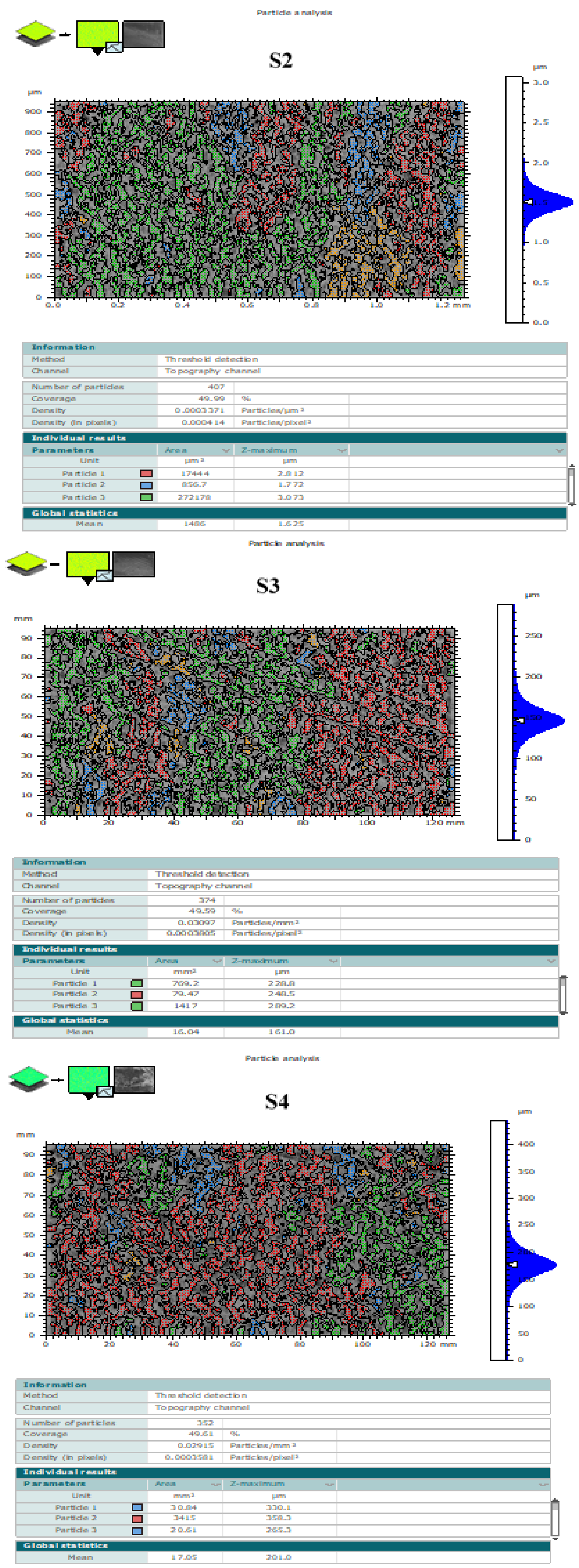

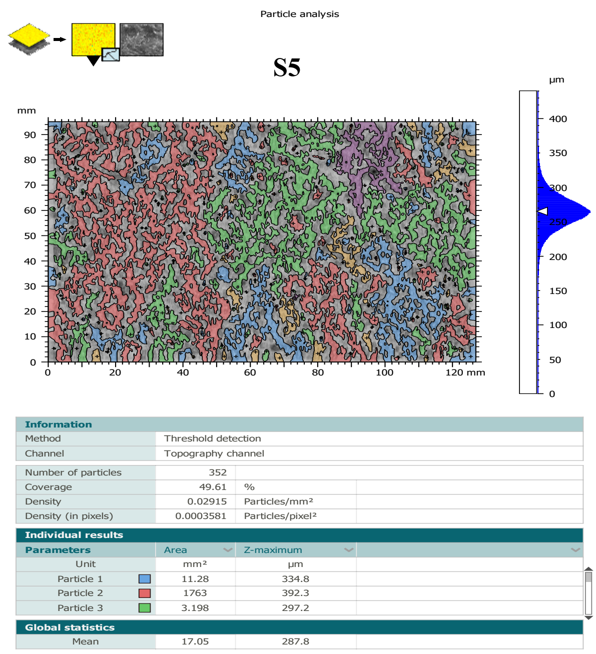

Figure 11. Particle analysis of SLA 3D- printed standard resin composites reinforced with CFP.

4. Conclusions

This study systematically investigated the effect of CFP concentration on the mechanical, surface and microstructural behavior of SLA 3D-printed photopolymer composites. The results demonstrated that CFP content plays a critical role in governing the balance between strength enhancement and structural integrity. Tensile analysis revealed that an intermediate reinforcement range of 0.125-0.25 wt% (S2-S3) provides the most balanced performance, achieving tensile strength of 10.28-11.82 MPa and higher ductility of 14.34-16.57%, along with maximum load capacity up to 565.72 N. In contrast, higher CFP loadings (S4-S5) increased tensile strength up to 13.04 MPa but resulted in reduced strain (9.71-12.41%), indicating increased brittleness and reduced plastic deformation capability. Hardness results showed a continuous improvement with increasing CFP content, rising from 47.50 HD (S1) to 58.00 HD (S5), confirming enhanced surface resistance due to reinforcement effects. Surface roughness analysis indicated a non-linear trend, where the highest fiber loading (S5) achieved the lowest Ra value (2.66 µm), suggesting improved surface smoothness; however this was accompanied by evidence of subsurface structural damage. SEM and particle analysis further confirmed that low reinforcement levels promote uniform particle distribution and stable microstructure, whereas higher CFP concentrations induce microvoids, uneven layer formation, brittle fracture features and internal cracking. Notably, S1 exhibited homogeneous particle dispersion, while S5 showed elevated particle density and maximum Z-max values (287.8 nm), indicating significant subsurface defects. Overall, the optimal CFP content range of 0.125-0.25 wt% ensures superior mechanical integrity, balanced ductility and acceptable surface quality due to effective stress transfer and uniform dispersion. Higher loading levels, although improving hardness and apparent surface finish, compromise structural reliability due to defect formation and interfacial weakness. Future research should focus on real-time process monitoring, fatigue and durability assessment, hybrid reinforcement strategies and multiscale modeling approaches to further enhance the reliability of SLA-fabricated fiber-reinforced composites for advanced engineering applications in automotive and biomedical sectors.

References

[1] M. Üstündağ and M. Kır, "Polymer additive manufacturing in stereolithography (SLA) and masked stereolithography (mSLA) methods: a review of advantages, limitations, and current applications," Gümüşhane Üniversitesi Fen Bilimleri Enstitüsü Dergisi, vol. 15, no. 4, pp. 1291–1306, Dec. 2025, doi: 10.17714/gumusfenbil.1593073.

[2] A. Husna, S. Ashrafi, A. A. Tomal, N. T. Tuli, and A. B. Rashid, "Recent advancements in stereolithography (SLA) and their optimization of process parameters for sustainable manufacturing," Hybrid Advances, vol. 7, p. 100307, Oct. 2024, doi: 10.1016/j.hybadv.2024.100307.

[3] J. Wong, A. Altassan, and D. W. Rosen, "Additive manufacturing of fiber-reinforced polymer composites: A technical review and status of design methodologies," Composites Part B Engineering, vol. 255, p. 110603, Feb. 2023, doi: 10.1016/j.compositesb.2023.110603.

[4] B. Pszczółkowski and M. Zaborowska, "Effect of layer exposure time in SLA-LCD printing on surface topography, hardness and chemical structure of UV-Cured photopolymer," Lubricants, vol. 13, no. 9, p. 406, Sep. 2025, doi: 10.3390/lubricants13090406.

[5] E. Hozdić, "Characterization and comparative analysis of mechanical parameters of FDM- and SLA-Printed ABS materials," Applied Sciences, vol. 14, no. 2, p. 649, Jan. 2024, doi: 10.3390/app14020649.

[6] P. Jirků et al., "Evaluation of mechanical properties and filler interaction in the field of SLA Polymeric Additive manufacturing," Materials, vol. 16, no. 14, p. 4955, Jul. 2023, doi: 10.3390/ma16144955.

[7] C. Yang, K. Wang, J. Zhang, and A. Codolini, "Additive manufacturing of Fibre-Reinforced polymer composites," Polymers, vol. 17, no. 12, p. 1652, Jun. 2025, doi: 10.3390/polym17121652.

[8] T. Gao et al., "Study on the reinforcement mechanism of LCD photopolymerization 3D-printed triply periodic minimal surface structures doped with carbon fiber and hydroxyapatite," Polymer Testing, vol. 156, p. 109134, Feb. 2026, doi: 10.1016/j.polymertesting.2026.109134.

[9] K. Rithika and J. Sudha, "Additive Manufacturing of Fiber-Reinforced Composites—A Comprehensive Overview," Polymers for Advanced Technologies, vol. 35, no. 12, Dec. 2024, doi: 10.1002/pat.70002.

[10] R. Xiao, M. Ding, Y. Wang, L. Gao, R. Fan, and Y. Lu, "Stereolithography (SLA) 3D printing of carbon fiber-graphene oxide (CF-GO) reinforced polymer lattices," Nanotechnology, vol. 32, no. 23, p. 235702, Feb. 2021, doi: 10.1088/1361-6528/abe825.

[11] M. Ramesh, K. Niranjana, R. Bhoopathi, and L. Rajeshkumar, "Additive manufacturing (3D printing) technologies for fiber-reinforced polymer composite materials: A review on fabrication methods and process parameters," e-Polymers, vol. 24, no. 1, Jan. 2024, doi: 10.1515/epoly-2023-0114.

[12] R. Wagmare, R. Harshe, J. Pednekar, and T. U. Patro, "Additive manufacturing of continuous fiber-reinforced polymer composites: current trend and future directions," Progress in Additive Manufacturing, vol. 10, no. 4, pp. 1973–2000, Sep. 2024, doi: 10.1007/s40964-024-00777-9.

[13] M. M. Rahman et al., "Polymer composites in Additive Manufacturing: Current technologies, applications, and emerging trends," Polymers, vol. 18, no. 2, p. 192, Jan. 2026, doi: 10.3390/polym18020192.

[14] C. Thomas and A. H. Sakhaei, "Additive manufacturing of continuous fibre reinforced composites: process, characterisation, modelling, and sustainability," Advanced Engineering Materials, Apr. 2026, doi: 10.1002/adem.202503048.

[15] R. M. Salih, A. Kadauw, H. Zeidler, and R. Aliyev, "Investigation of LCD 3D printing of carbon fiber composites by utilising central composite design," Journal of Manufacturing and Materials Processing, vol. 7, no. 2, p. 58, Mar. 2023, doi: 10.3390/jmmp7020058.

[16] G. Taormina, C. Sciancalepore, M. Messori, and F. Bondioli, "3D printing processes for photocurable polymeric materials: technologies, materials, and future trends," Journal of Applied Biomaterials & Functional Materials, vol. 16, no. 3, pp. 151–160, Apr. 2018, doi: 10.1177/2280800018764770.

[17] F. Tamburrino, B. Aruanno, A. Paoli, A. V. Razionale, and S. Barone, "Design and effect of a resin infiltration method to enhance the interlayer adhesion of additively manufactured PEEK parts," Polymers, vol. 17, no. 21, p. 2819, Oct. 2025, doi: 10.3390/polym17212819.

[18] J. Yan et al., "Improving mechanical and tribological properties of carbon fabric/resin laminated composites by carbon fiber powder," Polymer Composites, vol. 45, no. 5, pp. 4389–4400, Feb. 2024, doi: 10.1002/pc.28068.

[19] W. T. Nugroho, D. A. Tyagita, A. Wahyudiono, and D. D. Suranto, "DIMENSIONAL ACCURACY OF 3D PRINTED DOG BONE STRUCTURES," DOAJ (DOAJ: Directory of Open Access Journals), Aug. 2025, doi: 10.21776/jrm.v16i2.2158.